Reliable determination of *Prorocentrum micans* Ehrenb. (Prorocentrales, Dinophyceae) based on newly collected material from the type locality

Urban Tillmann, Mona Hoppenrath & Marc Gottschling

🗎 View supplementary material 🗗

📅 Published online: 13 May 2019.

✎ Submit your article to this journal 🗗

📊 Article views: 52

🔍 View related articles 🗗

View Crossmark data 🗗

British Phycological Society
Understanding and using algae

Taylor & Francis
Taylor & Francis Group

Check for updates

Reliable determination of *Prorocentrum micans* Ehrenb. (Prorocentrales, Dinophyceae) based on newly collected material from the type locality

Urban Tillmann [a], Mona Hoppenrath[b] and Marc Gottschling [c]

[a]Alfred Wegener Institut, Helmholz-Zentrum für Polar- und Meeresforschung, Am Handelshafen 12, D – 27570 Bremerhaven, Germany; [b]Senckenberg am Meer, German Centre for Marine Biodiversity Research (DZMB), Südstrand 44, D – 26382 Wilhelmshaven, Germany; [c]Department Biologie, Systematische Botanik und Mykologie, GeoBio-Center, Ludwig-Maximilians-Universität München, Menzinger Str. 67, D – 80638 München, Germany

ABSTRACT
The Prorocentrales are a unique group of dinophytes based on several apomorphic traits, but species delimitation is challenging within the group. The type species of *Prorocentrum*, namely *P. micans*, cannot be determined unambiguously, as important characters are not preserved in the original material collected in the first half of the 19th century. Water samples were taken at the type locality of *P. micans* in the Baltic Sea off Kiel (Germany) and strains with a morphology consistent with the protologue were established. An in-depth morphological analysis was performed, illustrating minute traits such as the periflagellar platelets and three different types of thecal pores. rRNA sequence data allowed for molecular characterization of the species. The newly collected material of *P. micans* was used for epitypification with the result that the type species of *Prorocentrum* can now be determined unambiguously.

Introduction

The Prorocentrales are a unique group of dinophytes, in which cingulum and sulcus are absent and the flagella are inserted apically (desmokont flagellation: Dodge, 1975; Fensome *et al.*, 1993; Murray *et al.*, 2009; Hoppenrath *et al.*, 2013). The theca consists of two large, lateral thecal plates, separated by a sagittal suture, and a cluster of small, periflagellar platelets surrounding two large pores, one of which is the flagellar pore (prorocentroid tabulation: Fensome *et al.*, 1993; Hoppenrath *et al.*, 2013). The platelets of the periflagellar area, and their associated structures, are diverse and probably species-specific (Hoppenrath *et al.*, 2013). Despite the distinct morphology, the Prorocentrales lineage has rarely been shown to be monophyletic in molecular phylogenetics, if a broad dinophyte taxon sample is used (Murray *et al.*, 2009; Orr *et al.*, 2012; Gu *et al.*, 2013; Bachvaroff *et al.*, 2014).

Prorocentrum micans Ehrenberg is one of the best known and most widely distributed dinophycean species (Dodge, 1975). It is marine and mainly neritic and has been globally recorded along the coasts of the northern Pacific and of the Atlantic in the northern and southern hemisphere, the Baltic Sea and the Mediterranean Sea (Ehrenberg, 1836; Bergh, 1881; Stein, 1883; Paulsen, 1907; Lohmann, 1908; Lebour, 1925; Braarud & Rossavik, 1951; Biecheler, 1952; Silva, 1959; Abé, 1967; Dodge, 1982; Paulmier,

1992; Cohen-Fernandez *et al.*, 2006; Hoppenrath *et al.*, 2009; Omura *et al.*, 2012; Han *et al.*, 2016). *Prorocentrum micans* is also found in the Arctic (Okolodkov, 1998; Caroppo *et al.*, 2017) but, to the best of our knowledge, there are no records from the Antarctic Ocean. The species is well known for usually non-toxic blooms in many coastal areas of the world (Braarud & Rossavik, 1951; Cassie, 1981; Pitcher & Calder, 2000), and maximum densities of up to 20 million cells per litre have been reported (Braarud & Heimdal, 1970). Some *P. micans* blooms have been described as noxious, affecting shellfish (Shumway, 1990), but these negative effects are due more to low oxygen availability. A few early reports on *P. micans* producing toxins (Pinto & Silva, 1956) are doubtful and have never been confirmed.

Ecologically, *P. micans* is mixotrophic (Jacobson & Anderson, 1996; Jeong *et al.*, 2005) and feeds myzocytotically with a peduncle (Schnepf & Winter 1990). The cells are easy to cultivate and, thus, there are numerous studies of *P. micans* regarding growth requirements (Kain & Fogg, 1960), clonal variability in growth rate (Brand, 1985), use of dissolved organic compounds (Mahoney & McLaughlin, 1977), taxis and migration (Hasle, 1950; Eggersdorfer & Häder, 1991), allelochemical interactions (Uchida, 1977; Jin *et al.*, 2005), population genetic diversity (Shankle *et al.*, 2004), ultrastructure (Dodge & Bibby, 1973; Schnepf &

Published online 13 May 2019

Winter, 1990; Roberts *et al.*, 1995) and life-history (Braarud & Rossavik, 1951; Bhaud *et al.*, 1988).

Prorocentrum micans is the type of *Prorocentrum* Ehrenberg (ICZN Art. 13.4.) and of the Prorocentrales, and is amongst the first 20 scientific names ever introduced in the dinophytes. The species was described by Ehrenberg (1835), who observed it in water tow samples from the Kiel Fjord (Baltic Sea, Germany) collected by the amateur naturalist G.A. Michaelis in September 1832 (Ehrenberg, 1836). Christian G. Ehrenberg's minute

water-colour drawings show cells exhibiting chloroplasts and with an outline that is asymmetrically obovate with acute antapex and a spine at the apex. The length of the cells is documented as ~60 μm, and Ehrenberg (1835) was unsure whether the species was bioluminescent. Kusber *et al.* (2005) inspected the original material including a mica of *P. micans* (preparation No. 540164-1, BHUPM) and lectotypified the taxon based on a cell (illustrated as their figs 2–4) in a lower ring marking a number of cells. However, this material is not informative in
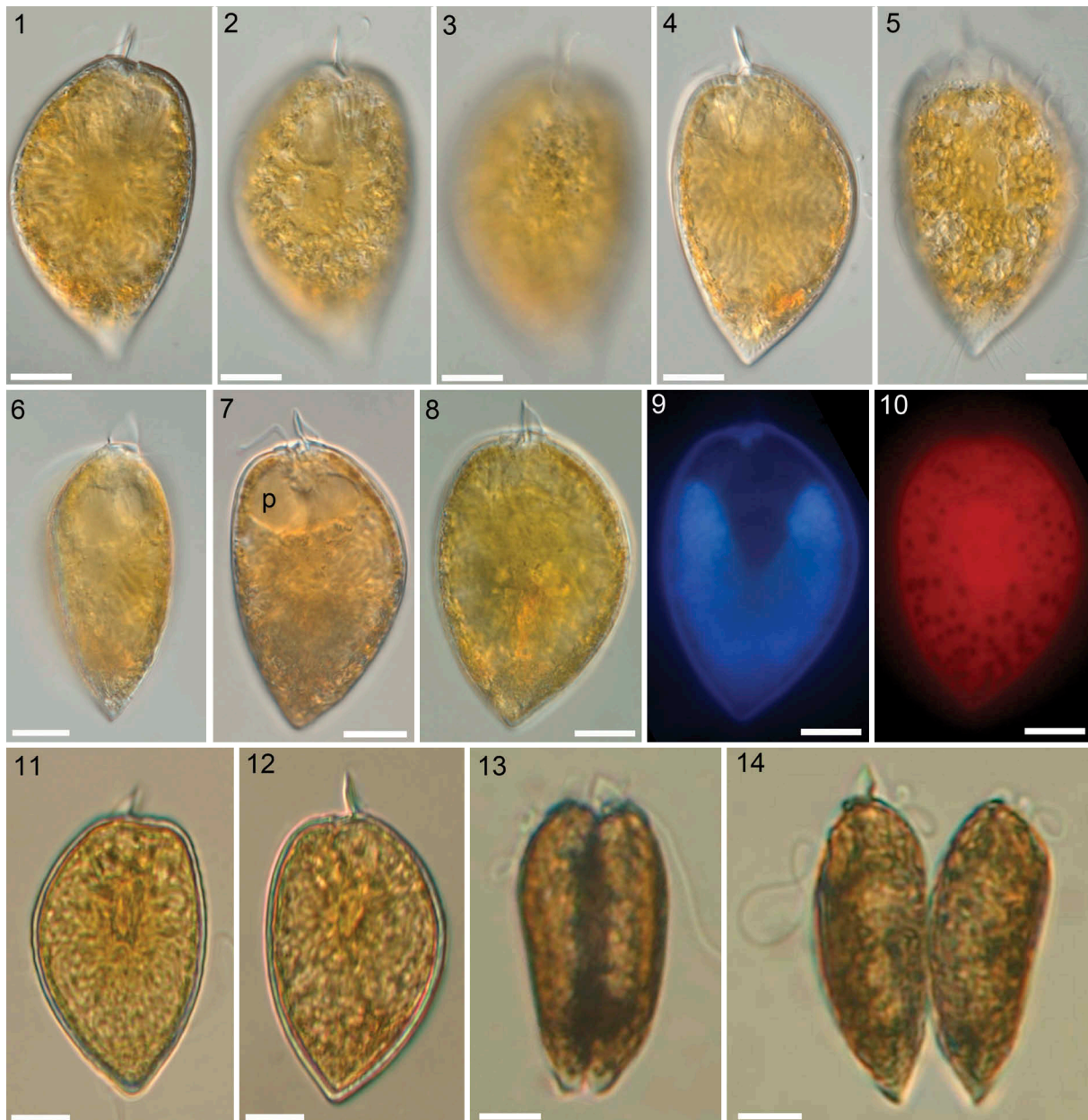
Figs 1–14. *Prorocentrum micans* (strain A10, LM). **Figs 1–7, 13, 14.** Living cells. **Figs 8–10.** Formalin-fixed cell. **Figs 11, 12.** Lugol-fixed cells. **Figs 1–7.** General size and shape of cells in lateral view of the right thecal plate (Figs 1–3), the left thecal plate (Figs 4, 5, 7, 8) and in ventral view (Fig. 6). Note the large apical trichocyst rods in Fig. 2, the poroid surface structure in Fig. 3, the thick chromosomes visible in Fig. 4, the radiating extruded trichocysts visible in Fig. 5, and the presumptive pusule (p) in Fig. 7. **Figs 8–10.** The same formalin-fixed cell stained with DAPI in brightfield (Fig. 8), with UV excitation (Fig. 9) to illustrate shape and position of the nucleus, and with blue light excitation (Fig. 10), when chlorophyll autofluorescence indicated chloroplast structure. **Figs 11, 12.** Right (Fig. 11) and left (Fig. 12) thecal plate of Lugol-fixed cells. Note the central, darkly stained area. **Figs 13, 14.** Ventral view of two stages during cell division. Scale bars = 10 μm.

terms of morphological details (e.g. pore types and their distribution at the cell surface, microarchitecture of periflagellar platelets) and of DNA sequence data.

Because of limited information, the original material of *P. micans* is ambiguous and the species can therefore not be critically identified for purposes of the precise application of the name (ICN Art. 9.9). Many species of *Prorocentrum* can be easily confused (Dodge, 1975; Lin *et al.*, 2006; Nagahama *et al.*, 2011; Hoppenrath *et al.*, 2013; Herrera-Sepúlveda *et al.*, 2015; Gómez *et al.*, 2017), and DNA sequence information is particularly essential in this group for reliable determination. Morphologically, *P. micans* has been considered to be very variable (Braarud & Rossavik, 1951; Bursa, 1959; Dodge, 1975) and the delimitation from similar species such as *Prorocentrum gracile* F.Schütt, *Prorocentrum triestinum* J.Schiller or *Prorocentrum mexicanum* Osorio-Tafall might be unclear (Taylor, 1976; Faust *et al.*, 1999; Hernández-Becerril *et al.*, 2000; Cohen-Fernandez *et al.*, 2006). Moreover, *Prorocentrum texanum* var. *cuspidatum* Henrichs, Steidinger, P.S. Scott & L.Campbell described in 2013 (Henrichs *et al.*, 2013) is genetically distinct but morphologically similar to *P. micans*. The same applies to the recently described species *Porocentrum koreanum* M.S.Han, S.Y.Cho & P.Wang (Han *et al.*, 2016), which is very similar if not indistinguishable from Ehrenberg's species, despite distinct genetic differences from strains listed as *P. micans*. In light of such uncertainties, the present study follows an epitypification approach (ICN Art. 9.8; Day *et al.*, 2010) that has turned out to be taxonomically useful for historical scientific names in dinophytes (Kretschmann *et al.*, 2015, 2018; Tillmann *et al.*, 2017). New material of *P. micans* was collected at the type locality in the Baltic Sea off Kiel and the present study aimed at the reliable determination of this ecologically and taxonomically important species.

Materials and methods

Sampling, cell isolation, cultivation

A surface water sample (temperature: 13.7°C, salinity: 15) was taken at the Kiel Fjord (Baltic Sea off Germany) from a harbour pier (54°20′41.0″N, 10°09′21.5″E) with a bucket on 20 October 2017. Single cells (exhibiting a morphology consistent with *Prorocentrum*) were isolated by micro-capillary into 96-well plates filled with 0.2 ml filtered water from the sample site. Plates were incubated at 15°C under 50 µmol photons m^{-2} s^{-1} on a 16:8 h light:dark photocycle in a controlled environment growth chamber (Sanyo Biomedica MIR 252; Wood Dale, Illinois, USA.

A total of 12 clonal strains of *P. micans* (Table 1) were established and cultivated in the conditions described above. Six of them were grown in natural seawater medium consisting of sterile filtered (0.2 µm VacuCap filters; Pall Life Sciences; Dreieich, Germany) and diluted North Sea water with a salinity of 15, and the other group of six strains in a full saline (salinity 33)

Table 1. Cell dimensions of 12 *Prorocentrum micans* strains grown in a salinity of either 15 or 33.

Strain	Salinity	Length (µm) mean ± SD min–max	Depth (µm) mean ± SD min–max	L/D ratio mean ± SD min–max	Posterior angle (°) mean ± SD min–max	N
A4	15	**49.6**±1.6 44.4–53.8	**30.5**±1.4 26.8–33.4	**1.63**±0.05 1.52–1.79	**80.8**±5.0 61.3–93.9	75
A10	15	**48.8**±1.6 40.5–51.9	**29.6**±1.4 24.4–32.4	**1.65**±0.06 1.50–1.78	**82.1**±6.0 68.8–109.8	87
B8	15	**50.5**±2.0 43.1–55.1	**29.7**±1.3 26.3–32.3	**1.70**±0.06 1.54–1.89	**80.1**±6.2 69.9–109.3	73
B11	15	**50.6**±1.8 42.9–53.6	**30.1**±1.5 26.9–33.0	**1.68**±0.06 1.55–1.86	**81.8**±6.3 66.2–109.4	75
C8	15	**48.1**±2.0 41.8–51.3	**29.0**±1.2 26.2–31.7	**1.66**±0.06 1.52–1.79	**82.3**±6.4 66.4–99.4	74
D10	15	**48.4**±1.5 43.0–53.3	**29.1**±1.2 25.2–31.3	**1.67**±0.05 1.56–1.86	**83.6**±4.7 73.7–99.5	72
A3	33	**53.6**±1.6 49.8–58.0	**31.2**±1.2 29.0–34.8	**1.72**±3.8 1.71–1.61	**76.7**±3.8 66.4–85.7	83
B1	33	**52.3**±1.7 49.1–55.8	**32.2**±1.5 29.0–35.7	**1.63**±0.04 1.56–1.72	**81.5**±3.6 72.3–89.3	70
B3	33	**52.3**±1.5 48.3–54.9	**31.1**±1.1 28.6–33.4	**1.68**±0.04 1.60–1.78	**77.2**±3.4 69.6–91.4	73
C3	33	**51.5**±1.4 48.2–54.7	**30.7**±1.0 28.3–33.7	**1.68**±0.04 1.57–1.81	**78.6**±3.8 71.8–91.0	86
D3	33	**51.9**±1.8 46.4–56.4	**32.1**±1.6 26.4–35.9	**1.62**±0.05 1.53–1.76	**85.3**±4.7 72.6–94.9	78
D6	33	**52.9**±1.5 50.1–58.2	**31.4**±1.0 28.8–34.5	**1.69**±0.04 1.60–1.84	**76.6**±3.8 65.3–88.1	82

For a sketch on how morphometric size measurements were performed see Supplementary fig. S1A. Note that all strains sequenced (i.e. A10, B11, D10) are identical with respect to their rRNA sequence.

seawater medium. Both salinity media were enriched with nutrients corresponding to 50% of K-medium (Keller *et al.*, 1987) slightly modified by omitting ammonium ions.

For DNA harvest, cells were collected by centrifugation (Eppendorf 5810R; Hamburg, Germany) in 50 ml centrifugation tubes at 3220×*g* for 10 min. Cell pellets were transferred to 1 ml microtubes, then again centrifuged (Eppendorf 5415, 16000×*g*, 5 min) and stored frozen (−20°C) for subsequent DNA extraction. In addition, all strains were grown and harvested as described above for lipophilic toxin analysis and stored at −20°C until use. For each harvest, cell density was determined by settling Lugol-fixed samples and counting >800 cells under an inverted microscope.

Microscopy

Observation of living or fixed cells (formaldehyde: 1% final concentration, or neutral Lugol-fixed: 1% final concentration) was carried out using an inverted microscope (Axiovert 200M; Zeiss; Munich, Germany) and a compound microscope (Axiovert 2; Zeiss), both equipped with epifluorescence and differential interference contrast optics. The shape and location of the nucleus was determined after staining of formalin-fixed cells with 4′-6-diamidino-2-phenylindole (DAPI, 0.1 µg ml^{-1} final concentration) for 10 min. Images were taken either with a digital camera (Axiocam MRc5; Zeiss), or videos were recorded using a digital camera (Gryphax Jenoptik; Jena, Germany) at full-HD resolution. Single frame micrographs were then extracted using Corel Video Studio software (Version X8, Coral; Ottawa, Canada).

Length and width of freshly fixed cells (neutral Lugol) from dense but healthy and growing strains (based on stereomicroscopic inspection of the living material) during late exponential phase were measured at microscopic magnification of 640× (1000× for spine length) using the inverted microscope and the Axiovision software (Zeiss). A detailed sketch on how morphometric size measurements were performed is provided as supplementary material (Supplementary fig. S1).

For scanning electron microscopy (SEM), cells were collected by centrifugation (Eppendorf 5810R; 3220×*g* for 10 min) from 15 ml of the strain. The supernatant was removed and the cell pellet re-suspended in 60% ethanol prepared in a 2 ml microtube with seawater (final salinity ~13) at 4°C for 1 h in order to strip off the outer cell membrane. Cells were further collected by centrifugation (Eppendorf 5415R; 16000×*g* for 5 min) and re-suspended in a 60:40 mixture of deionized water and seawater (final salinity ~13) at 4°C for 30 min. After centrifugation and removal of the diluted seawater supernatant, cells were fixed with formaldehyde (2% final concentration in a 60:40 mixture of deionized water and seawater)

and stored at 4°C for 3 h. Alternatively, cells were treated with TritonX (Sigma-Aldrich; St. Louis, Missouri, USA) at 0.5 % final concentration for 3 h.

Cells from both treatments were collected on polycarbonate filters (Millipore Merck; Darmstadt, Germany; 25mm Ø, 3 mm pore-size) in a filter funnel, in which all subsequent washing and dehydration steps were carried out. A total of eight washing steps (2 ml MilliQ-deionized water each) were followed by a dehydration series in ethanol (30%, 50%, 70%, 80%, 95%, 100%; 10 min each). Filters were dehydrated with hexamethyldisilazane (HMDS), first in 1:1 HMDS:EtOH, followed by twice 100% HMDS, and then stored in a desiccator under gentle vacuum. Finally, filters were mounted on stubs, sputter coated (Emscope SC500; Ashford, UK) with gold-palladium and viewed at 10 kV under a SEM (FEI Quanta FEG 200; Eindhoven, the Netherlands). Micrographs were presented on a black background using Photoshop 6.0 (Adobe Systems; San Jose, California, USA).

Toxin analysis

Cell pellets were suspended in 500 µl methanol and subsequently transferred to a FastPrep tube containing 0.9 g lysing matrix D (Thermo Savant; Illkirch, France). The samples were homogenized by reciprocal shaking at maximum speed (6.5 m s^{-1}) for 45 s in a Bio101 FastPrep instrument (Thermo Savant). After homogenization, samples were centrifuged (Eppendorf 5415 R) at 16 100×*g* at 4°C for 15 min. The supernatant (400 µl) was transferred to a spin-filter (pore-size 0.45 µm; Millipore Ultrafree; Eschborn, Germany) and centrifuged for 30 s at 800×*g*. The filtrate was transferred to an autosampler vial and analysed by LC-MS-MS for the presence of okadaic acid as described in Krock *et al.* (2008).

DNA sequencing

Genomic DNA was extracted from fresh material using the Nucleo Spin Plant II Kit (Machery-Nagel; Düren, Germany). Various regions of the ribosomal RNA (rRNA) genes including the Internal Transcribed Spacers (ITSs) were amplified using primer pairs specified previously (Gu *et al.*, 2013) and following standard protocols (Gottschling & Plötner, 2004; Gottschling *et al.*, 2012).

Terminology

Terminology of cell orientation, designation of thecal plates and platelets and ornamentation follows Hoppenrath *et al.* (2013), but cell width is corrected towards cell depth (i.e. dorsoventral width). In the present study, terminology for measurements in the periflagellar area is defined for future unambiguous descriptions (Supplementary fig. S2). The term 'wing'

was often used in the older literature as part of the spine in planktonic species of *Prorocentrum*. In the new definitions proposed by Hoppenrath *et al.* (2013), 'wing' is used (in a strict sense) for a thecal projection of a periflagellar platelet being broader than high, and the spine of platelet 1 is here described as having a 'sail'. The term 'mucron' (i.e. small tooth; Cohen-Fernandez *et al.*, 2006) is used for a small posterior structure or extension of one of the lateral thecal plates of *Prorocentrum*.

Results

General morphology

Using light microscopy (LM), all 12 clonal strains were identical in terms of morphology. Strain A10 was selected for the epitype and will be described and depicted in detail (Figs 1–50; 53, 55, 56, 58). Cell size for all strains ranged from 40.4 to 58.2 µm in length and 24.4 to 35.9 µm in depth (Table 1), with strains grown at a salinity of 33 being slightly larger compared with strains grown at a salinity of 15. Mean size for strain A10 was 48.8 µm in length and 29.6 µm in depth. Motile cells had both a longitudinal and a wavy transverse flagellum arising from the apical periflagellar area. Dividing cells kept their motility, and division was by desmoschisis along the sagittal suture (i.e. the two large thecal plates were shared between the two daughter cells: Figs 13, 14).

Cells were strongly compressed laterally (Fig. 6) and in lateral view, they were asymmetrically obovate in outline and had a rounded or slightly truncated and/or indented anterior part and an acute posterior end (Figs 1–14). Both dorsal and ventral sides of the theca were convex with the broadest part of the cells in the upper half of the cell. The dorsal convexity was stronger, and the ventral side could appear nearly a plane (Fig. 11). The posterior angle was variable, ranging from 68.8° to 109.8° (Table 2). At the apex, cells terminated with a distinct apical spine of 6.4 ± 0.5 µm in length (Table 2). Light microscopy also revealed a conspicuous line of rod-shaped trichocysts with a length of ~7 µm visible in the apical area (Fig. 2) and a poroid surface of the theca (Fig. 3). Under a coverslip, living cells were regularly observed with extruded trichocysts radiating from the cell surface, especially in the posterior part (Fig. 5).

A large U- to V-shaped nucleus with thick, dinokaryotic chromosomes (Fig. 4) extended about 65% of the cell length (Fig. 9). Two lobed and retiform, brownish chloroplasts were parietally arranged (Figs 5, 10). No stalked pyrenoid with starch sheath was visible in LM. However, a densely stained area was observed in the centre of Lugol-fixed cells (Figs 11, 12), in which the

chloroplast seemed to lack perforations (Fig. 10). A large, round or bilobatedly kidney-shaped, hyaline area (presumably a pusule) was occasionally visible in the anterior part of the cell (Figs 6, 7).

Scanning electron microscopy confirmed the general appearance of the cell (Figs 15–31) and revealed the three-dimensional shape of both thecal plates in more detail (Figs 17–22). Moreover, a number of structural details could be demonstrated. The spine consisted of a broad spearhead-shaped part arranged perpendicular to the sagittal plane and it was slightly variable among individual cells (it also varied depending on the individual perspective in the microscope). On the left lateral side, the spine extended to the ventral side as a steeply narrowing sail oriented in the cell's sagittal plane (Figs 23–28). The total length of the spine (in SEM specimens) was 6.2 ± 0.6 µm (n = 11). Opposite the large spine, there was a small wing (Figs 23, 38).

At the posterior end of the cell, there was a small triangular extension of the theca (i.e. mucron) bent slightly upwards. However, the mucron was only present on the left thecal plate (Figs 29–31). Between the two thecal plates there was an intercalary band of varying width, which was densely striated transversally (0.4–0.7 µm between stripes, n = 15; Figs 17–20, 31, Supplementary fig. S7) and occasionally a few horizontal lines were also observed (Fig. 31, Supplementary fig. S7). In a few specimens the transition between intercalary band and theca was marked by a dense row of small, roundish depressions (Fig. 19).

The surface of both thecal plates was foveate with round or oval (or occasionally more kidney shaped and elongated) depressions with a density of $1.24 \pm 0.20 \ \mu m^{-2}$

Table 2. Morphometric measurements for *Prorocentrum micans* strain A10 as measured with light microscopy (LM) or scanning electron microscopy (SEM).

Trait	Mean ± SD	Min – Max	N
Length LM (µm)	48.8 ± 1.6	40.5 – 51.9	87
Depth LM (µm)	29.6 ± 1.4	24.4 – 32.4	87
L/D LM ratio	1.65 ± 0.06	1.50 – 1.78	87
Posterior angle LM (°)	82.1 ± 6.0	68.8 – 109.8	87
Spine length LM (µm)	6.4 ± 0.46	5.1 – 7.3	50
Large pore diameter SEM (µm)	0.66 ± 0.05	0.55 – 0.76	31
Small pore diameter SEM (µm)	0.18 ± 0.01	0.16 – 0.22	33
Mini pore diameter SEM (µm)	0.12 ± 0.01	0.11 – 0.13	20
Depression density SEM (µm^{-2})	1.24 ± 0.20	0.96 – 1.74	20
Depression area SEM (µm^2)	0.18 ± 0.08	0.02 – 0.49	500
Number large pores right plate SEM	76.0 ± 6.8	63 – 87	14
Number small pores right plate SEM	50.4 ± 5.1	42 – 63	13
Number large pores left plate SEM	78.0 ± 6.6	65 – 89	19
Number small pores left plate SEM	53.9 ± 8.3	39 – 75	19
Depth periflagellar area SEM (µm)	6.3 ± 0.5	5.0 – 7.6	25
Length periflagellar area SEM (µm)	3.4 ± 0.4	2.9 – 4.5	17
Width ap SEM (µm)	0.7 ± 0.1	0.6 – 0.9	7
Length ap SEM (µm)	1.3 ± 0.1	1.1 – 1.5	7
Width fp SEM (µm)	0.9 ± 0.1	0.8 – 1.1	14
Length fp SEM (µm)	1.7 ± 0.1	1.4 – 1.9	11

Abbreviations: L/D: length/depth; ap: accessory pore; fp: flagellar pore.
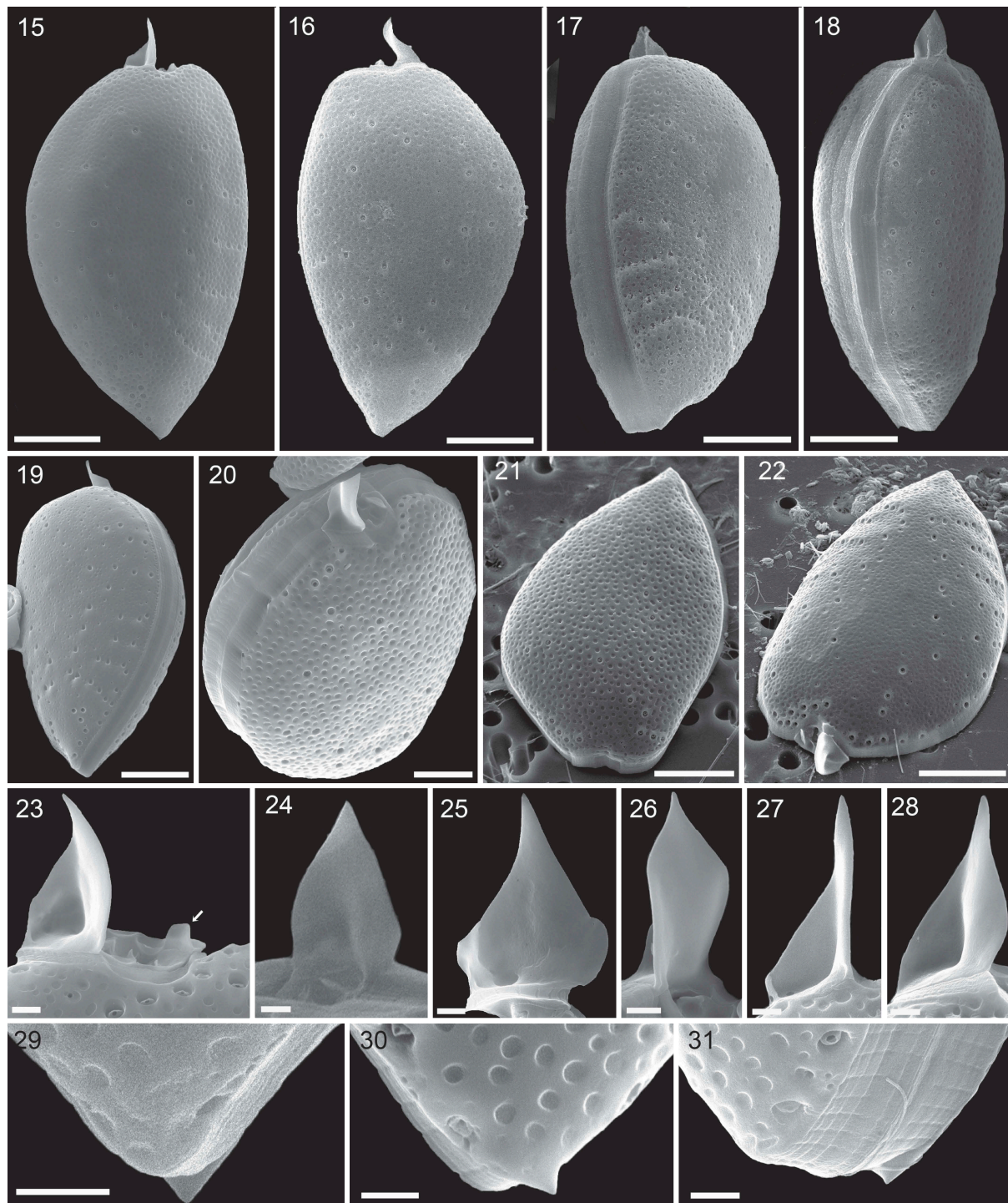
Figs 15–31. *Prorocentrum micans* (strain A10, SEM). **Figs 15–20.** Entire cells in right thecal view (Fig. 15), left thecal view (Fig. 16), ventral-lateral view (Fig. 17), dorsal-lateral view (Fig. 18), left thecal view (Fig. 19) and apical view (Fig. 20). **Figs 21, 22.** Left thecal plate (Fig. 21) and right thecal plate (Fig. 22) in apical view to illustrate three-dimensional shape of the thecal plates. **Figs 23–28.** Different views of the apical spine. Note the short wing (arrow in Fig. 23) opposite to the spine. **Figs 29–31.** Different views of the short, triangular posterior termination (mucron) on the left thecal plate. Scale bars = 10 μm (Figs 15–19, 21, 22), 5 μm (Fig. 20), 1μm (Figs 23–31).

(n = 20). The area of the depressions ranged from 0.02 to 0.49 μm^2 (Table 2). Presence and development of depressions seemed to depend on thecal age. Presumably, recently formed thecal plates were free of depressions (Figs 37, 40), and various developmental stages in size and depth of the depressions were observed (Fig. 19). Moreover, dorsal or ventral views (i.e. non-lateral views) revealed cells with markedly differing foveate ornamentation of both thecal plates (Fig. 38, Supplementary figs S4–S6).
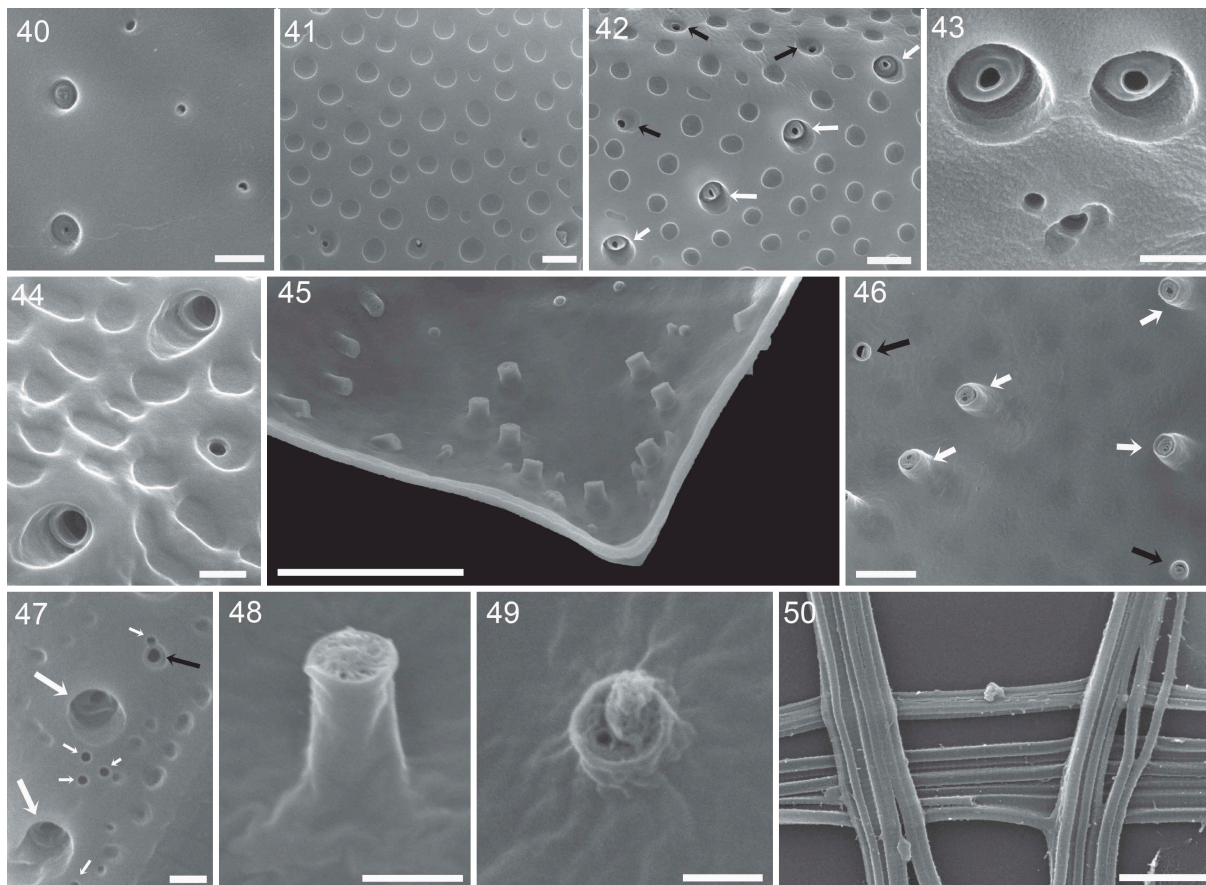
Thecal pores

There were three different types of thecal pore present. Firstly and most obviously, there were large trichocyst pores consisting of a large canal with an outer diameter of 0.66 ± 0.05 µm (n = 31). In the centre of the canal, a protuberance was visible with an inner opening either being very small (Figs 42, 43, Supplementary figs S8, S9) or wide (Fig. 44, Supplementary figs S10, S11), the latter probably representing the stage after trichocyst extrusion. From internal thecal views, the tubular structure of large trichocyst pores was discernible (Figs 35, 36, 45, 46); they extended for ~0.6 µm inside of the theca with an inner opening (although mainly covered by fibrous material in SEM preparations) of ~0.3 µm diameter (Fig. 48). Secondly, there were small pores present (Figs 40, 42) which predominantly were recessed and located in the centre of a round depression (Fig. 42). The opening of these small pores had a diameter of 0.18 ± 0.01 µm (n = 33). Internal theca view revealed that the small pores were also tubular but with a distinctly smaller inner extension (~0.07 µm) and inner diameter (~0.2 µm) (Figs 45, 46, 49). Finally, there was a third type of pore present, which was not located inside a depression and whose diameter was the smallest (0.11 to 0.13 µm, n = 20). These mini-pores were present on both thecal plates, were consistently restricted to the most posterior part of the cells, and they often formed small clusters (Fig. 47).

Large and small pores were abundant on both thecal plates (Table 2) with ~77 and 52 large and small pores per plate, respectively, leaving only an elongated, narrow central area free of pores. Large trichocyst pores were densest in the lower third of the thecal plates, where they were mainly arranged in radial rows around the margins (Figs 32–37, 51, 52). The two most posteriorly located rows of large pores were arranged in a semicircle. Upwards, there were
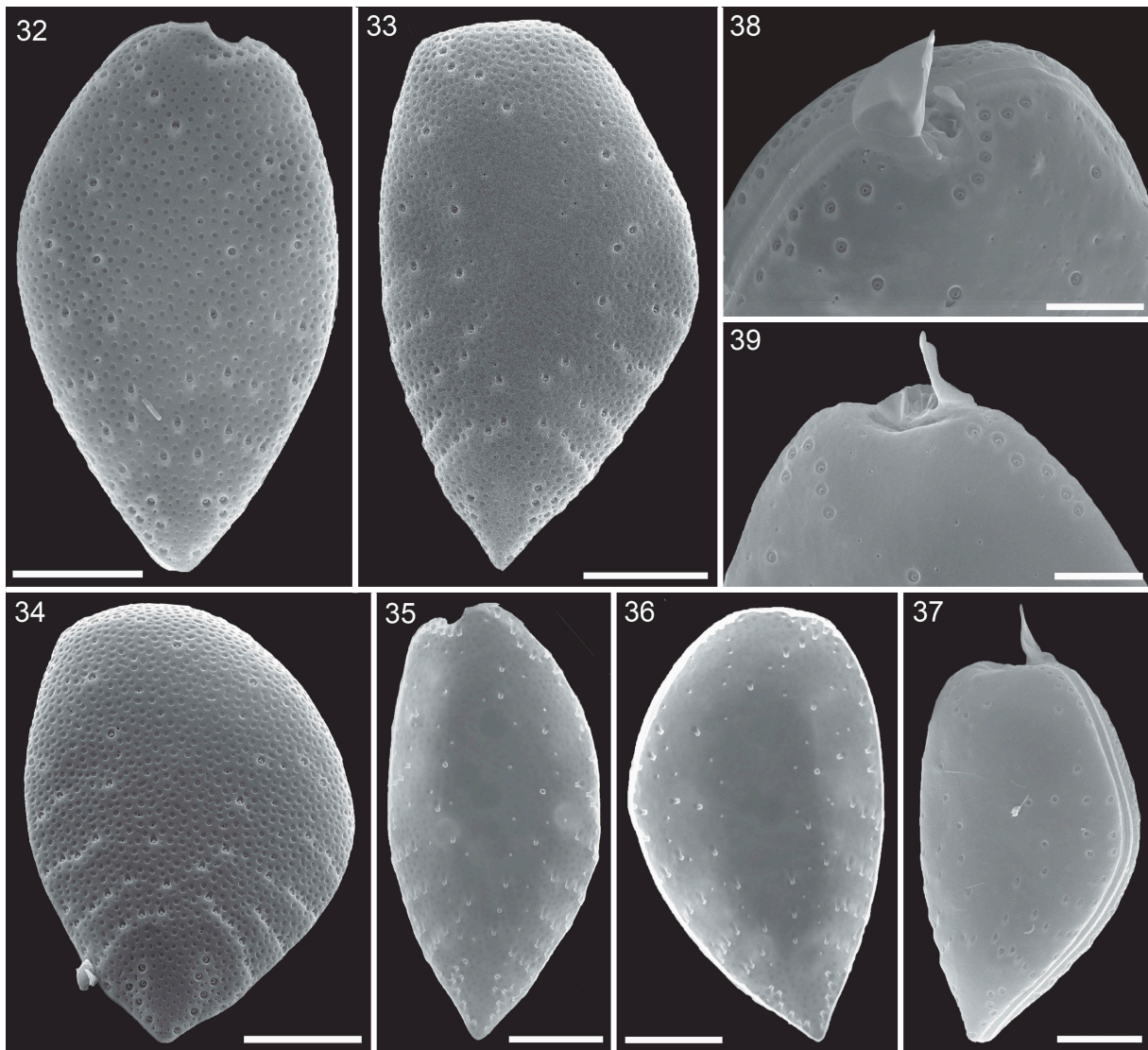
Figs 32–39. Surface structure and pore patterns of *Prorocentrum micans* (strain A10, SEM). **Fig. 32**. Right thecal plate. **Fig. 33**. Left thecal plate. **Fig. 34**. Left thecal plate in posterior view. **Fig. 35**. Right thecal plate in internal view. **Fig. 36**. Left thecal plate in internal view. **Fig. 37**. Entire cell with a presumably newly formed left thecal plate free of surface depressions. **Figs 38, 39**. Apical pore pattern of the right (Fig. 38) and left (Fig. 39) thecal plate. Scale bars = 10 µm (Figs 32–37) or 5 µm (Figs 38, 39).

Figs 40–50. Surface structure and pores of *Prorocentrum micans* (strain A10, SEM). **Fig. 40**. Smooth surface of a presumably newly formed thecal plate with large trichocyst pores on the left and small pores on the right side. **Fig. 41**. Detailed view of size and shape of the surface depressions (foveate ornamentation). **Fig. 42**. Large trichocyst pores (white arrows) and small pores (black arrows). **Fig. 43**. Detailed view of the fine structure of large trichocyst pores. **Fig. 44.** Two large trichocyst pores with a sloped opening. **Fig. 45**. Internal view of the posterior part of the left thecal plate showing tubular structure of thecal pores. **Fig. 46**. Detailed internal view with large trichocyst pores (white arrows) and small pores (black arrows). **Fig. 47**. Enlarged view of the posterior part of the thecal plate showing large trichoycst pores (large white arrows), a small pore (black arrow) and a few mini-pores (small white arrows). **Figs 48, 49**. Detailed internal view of a large trichocyst pore (Fig. 48) and a small pore (Fig. 49). **Fig. 50**. Bundles of extruded trichocysts showing the tetragonal and densely striated structure. Scale bars = 5 µm (45), 1 µm (Figs 40–42, 46, 50), 0.5 µm (Figs 43, 44, 47, 48), 0.2 µm (Fig. 49).

usually four rows of large pores on each side consisting of usually three to six pores per row. Occasionally, these rows were located in slightly recessed depressions leading to a somewhat serrated appearance of the theca (Figs 33, 34). In the lower half, but not for the most posterior part of the cell, the deep cavities of trichocyst pores usually had a flat angle slope pointing towards the anterior or lateral side of the cell (Figs 32, 34–37, 44).

In the apical area, large trichocyst pores formed some characteristic patterns. On the right theca, there was a winding row of usually eight pores (7–10, n = 30) starting just below the apical spine and following the anterior excavation to the ventral side of the cell (Fig. 38). On the dorsal side of the left plate, there was a row of usually six pores (5–7, n = 24) along the plate margin and starting dorsally from the spine. The area below the periflagellar area of the left plate was free of pores. The apical pore pattern of the dorsal right theca and of the ventral left theca were

more variable and basically consisted of a few pores along the margin and a few pores in an arched inwards running row (Figs 38, 39). In SEM preparation, extruded trichocysts were abundant. They were tetragonal, about 0.11 µm in width and had a very fine horizontal striation (Fig. 50).

Periflagellar area

The cell apex was formed by the periflagellar area, which was about 6 µm deep and 3 µm wide (Table 2). It fitted into place between both thecal plates in a gap with a long and drawn out bend of the left plate and an additional, broadly V-shaped, indentation of the right plate (Fig. 53). The periflagellar area was composed of nine platelets surrounding a flagellar pore (fp) and an accessory pore (ap) (Figs 54–61). One of the regular platelets (i.e. platelet 6) was consistently split into two parts (platelet formula: 1 2 3 4 5 6a, b 7 8). The fp was
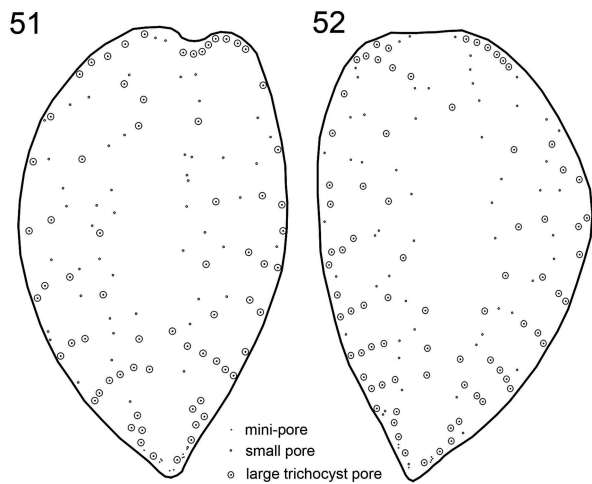
Figs 51, 52. Schematic drawing of a representative pore pattern of the right (Fig. 51) and left (Fig. 52) theca of *Prorocentrum micans* (strain A10).

irregular in shape, generally longer than wide in right lateral to apical view (~1.7 µm long, 0.9 µm wide, Table 2; for orientation see Supplementary fig. S1B) and surrounded by platelets 3, 5, 6b and 8. The ap was similar in shape but smaller (~1.3 µm long, 0.7 µm wide, Table 2) and surrounded by platelets 7 and 8. Both pores internally had additional lip-like structures (Figs 58, 59), forming a tubular and funnel-like extension into the cell (Fig. 55), which was also visible in LM with UV excitation (Fig. 9).

The triangular platelet 1 was the largest and carried the long spine with sail, whereas the triangular but distinctly smaller platelet 4 on the opposite edge of the periflagellar area supported a short (height: 0.8 ± 0.1 µm; range 0.6–1.1 µm; n = 15) wing (Figs 23, 38, 54, 56–58) running along almost all of the suture between platelet 4 and platelets 3 and 5 (width: 1.5 ± 0.3 µm, range 1.1–2.0 µm; n = 20). On the other platelets, very short, irregular platelet lists were present occasionally (Fig. 60). The number and arrangement of apical platelets of strain A10 were confirmed by SEM for two of the other Kiel Bight strains (i.e. B11, D11). Size and shape of single periflagellar platelets within the clonal materials were slightly variable (Supplementary figs S12–S24). For two cells, a variation in platelet configuration was observed, in which platelet 6a anomalously was in contact with platelet 1 (Supplementary figs S25, S26).

Molecular diagnostics

rRNA sequences of strains A10, B11 and D10 (Table 1) were deposited in GenBank as entries MK405477, MK405478, MK405479 and MK405480. The sequence of the strain A10 (i.e. from which the epitype was prepared) compared with other sequences assigned to

P. micans and to closely related species of *Prorocentrum* is shown in Fig. 62. Although not entirely identical, sequences associated with *P. micans* showed four autapomorphic (i.e. diagnostic) positions, delimiting it from all other species of *Prorocentrum* (including *P. koreanum*).

Toxins

All strains were negative for the presence of okadaic acid. Due to slightly different biomass available for different strains, the limit of detection varied between 3.1 and 5.2 fg cell^{-1}.

Discussion

Reliable determination of species is a necessary prerequisite for any applied research in ecology, biogeography and experimental biology. This is particularly true for taxonomically challenging groups such as protists, including *Prorocentrum* which is the focus of the present study. The original material of the type species, *P. micans*, in the Ehrenberg collection (BHUPM) provides information about the cell shape being obovoid, rounded anteriorly, acute posteriorly, more flattened ventrally and convex dorsally (Kusber *et al.*, 2005). The cells in Ehrenberg's drawings are somewhat more symmetrical than the physical cells available in micas. Preserved cells are 45.0–46.8 µm long (without spine) and 28.2–30.0 µm deep (n = 3) and a prominent, apical, 7.2–10.8 µm long (n = 3) spine with sail is present. The foveate ornamentation, with short rows of large pores, is likewise visible in the original material, but traits such as different pore-types and their distributions over the cell surface, or the microarchitecture of the periflagellar platelets are not preserved. Today, we know that these and other morphometric details are required for an unambiguous identification of closely related species of *Prorocentrum*. DNA sequence information is further important for the correct determination of species in the microbial world and the application of the name *P. micans* has thus been ambiguous (ICN Art. 9.9) prior to our study.

In cases of taxonomic ambiguity, the epitypification approach (Day *et al.*, 2010) has been successfully applied for historical scientific names in the past (Kretschmann *et al.*, 2015, 2018; Tillmann *et al.*, 2017). The clonal strain isolated from the type locality and documented here in much detail does not contradict the description and original material of *P. micans* (Ehrenberg, 1835; Kusber *et al.*, 2005). The cell size, shape, thecal ornamentation and apical spine morphology cannot be distinguished from the original material, although the apical spine is slightly shorter (Table 2). However, size ranges are overlapping and we are confident that, in fact, our material is correctly determined as *P. micans*. Thus, epitypification of *P. micans* (see below) is possible, justified and
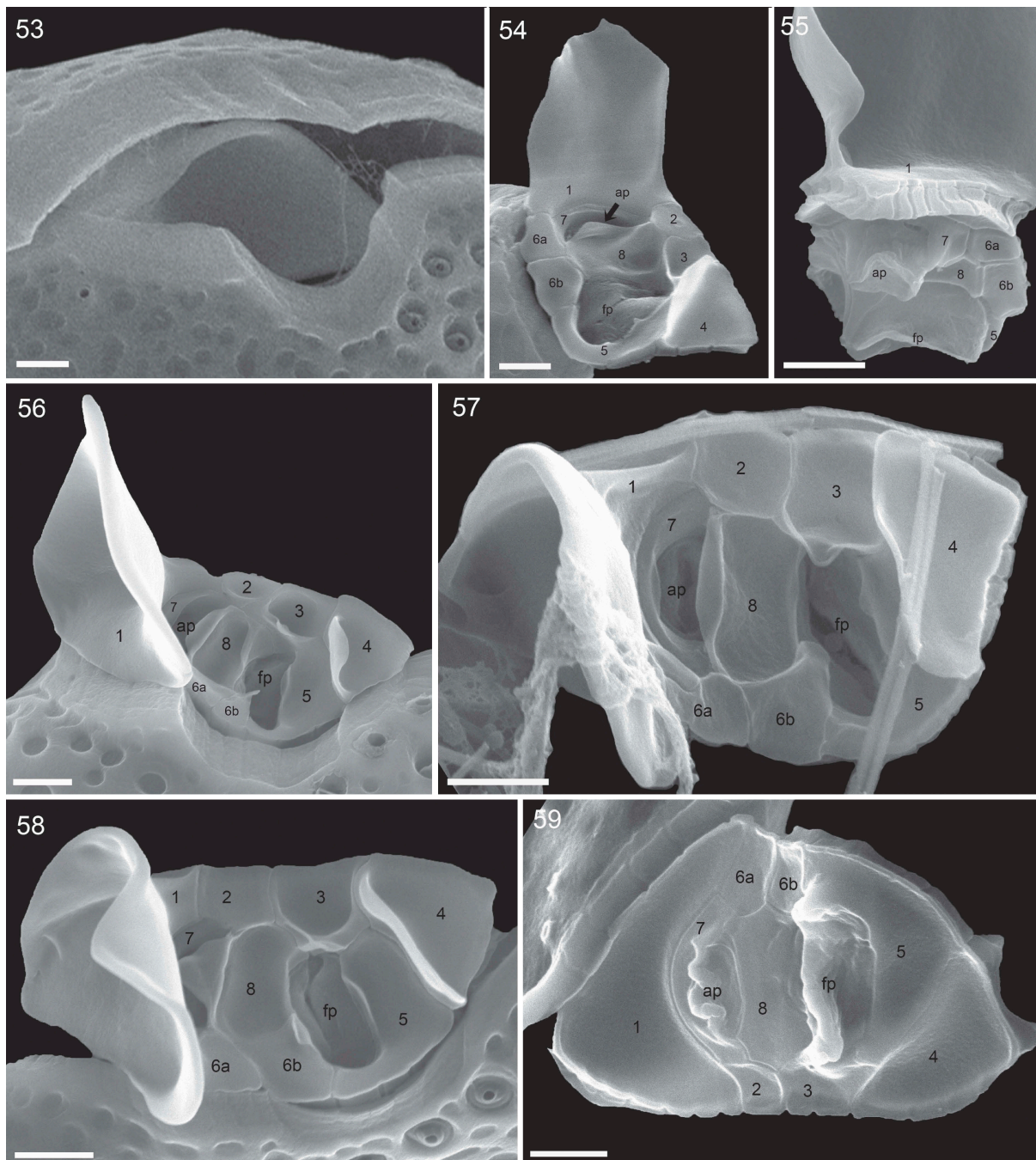
Figs 53–59. Periflagellar area of *Prorocentrum micans* (SEM). **Fig. 53.** Apical view of a cell (strain A10), whose periflagellar area was detached revealing the shape of the apical notch of both thecal plates. **Fig. 54.** Ventral apical view of the periflagellar area (strain D10). **Fig. 55.** Posterior dorsal view of a detached periflagellar area (strain A10) showing the internal extension of accessory and flagellar pore. **Figs 56–58.** Apical view of the periflagellar area (Figs 56, 58: strain A10; Fig. 57: strain B11). Note that in Fig. 58, a bent short list of platelet 8 is covering and hiding the accessory pore. **Fig. 59.** Internal view of the periflagellar area (strain B11). ap = accessory pore, fp = flagellar pore. Scale bars = 1 μm.

advised, and allows for adding morphological and molecular data to the species circumscription for unambiguous identifications in future.

In terms of morphology, information about the exact number and the arrangement of the periflagellar platelets is a striking addition made here. Such features are rarely reported for planktonic species of *Prorocentrum*, although they are considered crucial for a consistent taxonomy of Prorocentrales. Detailed

and reliable high magnification SEM images of the apical area are difficult to obtain and, therefore, a comparison with an early drawing of the periflagellar area of *P. micans* (Taylor, 1980; Fensome *et al.*, 1993) should be made with care. Twelve (instead of nine) platelets are depicted (Supplementary fig. S3), with a number of very small elements arranged around, or close to, the accessory pore (platelet formula: 1 2a, b 3 4 5 6a, b 7a, c 8a, c). The relative size and shape of,
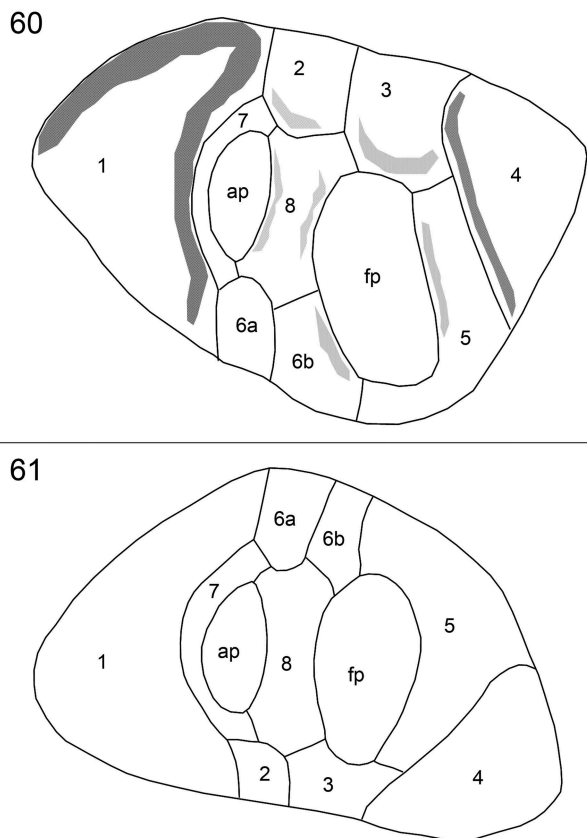
Figs 60, 61. Schematic drawings of the periflagellar area in external (Fig. 60) and internal (Fig. 61) view. ap = accessory pore, fp = flagellar pore.

for example, platelets 2 (with split and narrower), 3 (much deeper and larger) and 4 (much smaller) differ markedly from our observations (Figs 60, 61, Supplementary fig. S2). The periflagellar area (Taylor, 1980; Fensome et al., 1993) is inferred from stained light micrographs (provided by Hans A. von Stosch), and it remains to be clarified whether it represents a real and deviating platelet pattern (indicative of a potentially different species), or is based on preparation and/or observation artefacts. In any case, the present study indicates that the periflagellar platelet pattern is a suitable morphological trait, as stability and consistency for three clonal strains is shown. However, the number of micrographs with all plates unambiguously visible is still limited and size and shape of single platelets and, exceptionally, also the arrangement of one of the platelets (namely 6a) can vary within a clonal strain.

The presence of a mucron in the antapical thecal region is considered a diagnostic character for delimiting species or closely related species groups of *Prorocentrum*. In particular, the mucron of *P. gracile* (with *P. sigmoides* Böhm in synonymy) has been considered as a possible diagnostic character that should be evaluated based on further observations of material from different geographic regions (Cohen-Fernandez et al., 2006). We demonstrate the mucron also for *P.*

micans in the present study and, thus, its presence or absence appears to be a morphological trait at the group, rather than the species, level. The mucron is a tiny structure, and further investigations of strains and field material within the *P. micans* species complex will shed light on intra- and inter-specific variability of this trait and whether peculiar character states may turn out as diagnostic for species.

We are still searching for reliable morphological traits to distinguish between (closely related) species of *Prorocentrum* and to the best of our knowledge, the presence of minipores are here described for the first time. They are neither recognizable on SEM images published under the name *P. micans* nor on those of related species such as *P. gracile, P. koreanum* or *P. texanum* (Cohen-Fernandez et al., 2006; Henrichs et al., 2013; Han et al., 2016). High magnification microscopy is needed to observe minipores, and all species of *Prorocentrum* are in need of a rigorous re-investigation concerning this morphological trait. The same is true for the pore pattern, but this is difficult because there is no consistent descriptive terminology available at present. As a result, text and images or drawings can be occasionally confusing, and statements such as those which say the pore patterns (around the periflagellar area and the thecal surface) of *P. micans* and *P. koreanum* are 'very different' (Han et al., 2016, p. 40) are truly open for interpretation.

We now have at hand all information necessary to identify *P. micans* reliably and unambiguously and can start to compare *P. micans* with previous studies, some of which are based on large morphological data sets and/or extensive DNA sequence information (Cohen-Fernandez et al., 2006, 2010; Han et al., 2016). Moreover, we are enabled now to distinguish this taxon from other similar species of *Prorocentrum*, in particular from the recently described *P. koreanum* (Han et al., 2016). The species is clearly distinct from *P. micans* (identified by strain A10) as inferred from rRNA sequence data, but agrees to a large extent with the LM morphology of *P. micans* (a phenomenon termed cryptic speciation). In turn, a Korean strain determined as *P. micans*, and with rRNA sequence data very similar to our epitype barcode (and other strains listed as *P. micans*), is described as morphologically different from the material investigated in the present study (Han et al., 2016), but subsequent study with high-resolution SEM images must work out such differences in detail to clarify the situation. Future research is necessary to disentangle the complex taxonomy of species similar to *P. micans* and with the present study a crucial step forward has been made in this respect.

Epitypification

Prorocentrum micans Ehrenberg, Abhandlungen der Königlichen Akademie der Wissenschaften in Berlin 1833, Physikalische Klasse: 307–308. 1835. 1952. – Type [mica with non-fossil specimen]: Baltic Sea off
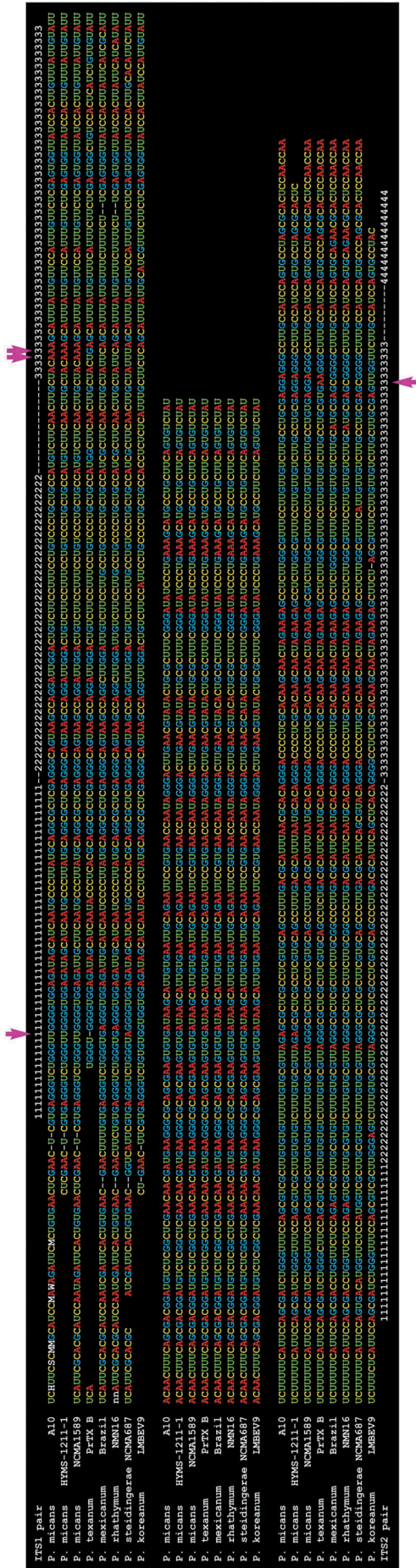
Fig. 62. Alignment of the full ITS sequences comprising *Prorocentrum micans* (3 strains, including A10, from which the epitype was prepared) and other closely related species of *Prorocentrum*. Internal Transcribed Spacer 1 (upper third), 5.8S rRNA (middle third) and Internal Transcribed Spacer 2 (lower third) are separated, and pairing regions (Gottschling & Plötner 2004) are indicated by numbers. Autapomorphic (i.e. diagnostic) positions of *Prorocentrum micans* are indicated by pink arrows.

Germany. Schleswig-Holstein, Kiel, Sep 1832 [prepared Nov 25 1832]: G.A. Michaelis [Ch.G. Ehrenberg] s.n. (lectotype, designated by Kusber *et al.* 2005 and illustrated as figs 2–4: BHUPM 540164-1); [SEM stub]: Baltic Sea off Germany. Schleswig-Holstein, Kiel, Oct 20, 2017: K.J.S. Meier [U. Tillmann] A10 (epitype, designated here: CEDiT2018E87) [http://phycobank. org/101001].

Note: Volume 1833 of the Abhandlungen was probably printed in 1834, but was not published before 1835 due to problems with the printing costs of the copper plates (*pers. comm.* St. Fölske, Archiv der Berlin-Brandenburgischen Akademie der Wissenschaften). The lectotypification of McLachlan *et al.* (1997) is to be subsumed, as the corresponding reference (Ehrenberg, 1836) was published after the protologue (Ehrenberg, 1835). Kusber *et al.* (2005) emphasized that the copper engravings are later interpretations of original material and are thus not eligible for typification purposes (ICN Art. 9.3).

Acknowledgements

Disclosure statement

No potential conflict of interest was reported by the authors.

Funding

Supplementary information

The following supplementary material is accessible via the Supplementary Content tab on the article's online page at http://10.1080/09670262.2019.1579925
Supplementary figs S1–S3: *Prorocentrum micans*, sketch on how morphometric size measurements were performed for cell dimensions (**Fig. S1**) and for the periflagellar area (**Fig. S2**). **Fig. S3**. Platelet pattern of *P. micans* as proposed by Fensome *et al.* (1993).
Supplementary figs S4–S11: Surface structure and pore patterns of *Prorocentrum micans* strain A10 (SEM). **Fig. S4**. Ventral view of a cell where the right plate is smooth and the left plate is foveate. **Figs S5, S6**. Apical area of cells

with one smooth and one foveate thecal plate. **Fig. S7**. Detailed view of a broad sagittal suture with a few vertical lines (arrows) next to the dense horizontal striation. **Figs S8–S11**. Examples of large trichocyst pores with the spinning-nozzle like structure visible with an inner opening either being very small (Figs S8, S9) or wide (Figs S10, S11). Scale bars = 5 µm (Figs S4–S6), 1 µm (Fig. S7), 0.5 µm (Figs S8–S11).

Supplementary figs S12–S24: Periflagellar area of *Prorocentrum micans* (SEM) in apical (Figs S12–S19) or internal (Figs S20–S24) view. Figs S13–S19, S23: strain A10; Figs S12, S20, S22, S24: strain B11; Fig. S21: strain D10. Note that only plates that are visible are labelled. ap = accessory pore, fp = flagellar pore. Scale bar = 1 µm.

Supplementary figs S25, S26: Periflagellar area of *Prorocentrum micans* (SEM). Variation in platelet configuration: platelet 6a anomalously in contact with platelet 1 (arrows). Fig. S25: strain B11, Fig. S26: strain A10. Scale bar = 1 µm.

Author contributions

U. Tillmann: isolation, culturing, LM and SEM, drafting and editing manuscript; M. Hoppenrath: *Prorocentrum* terminology, drafting and editing manuscript; M. Gottschling: original concept, analysis of molecular data, taxonomy, drafting and editing manuscript.

ORCID

Urban Tillmann http://orcid.org/0000-0002-8207-4382
Marc Gottschling http://orcid.org/0000-0002-4381-8051

References

Abé, T.H. (1967). The armoured Dinoflagellata: I. Prorocentridae and Dinophysidae (A). *Seto Sea Marine Biological Laboratory Publishers*, **14**: 369–389.

Bachvaroff, T.R., Gornik, S.G., Concepcion, G.T., Waller, R. F., Mendez, G.S., Lippmeier, J.C. & Delwiche, C.F. (2014). Dinoflagellate phylogeny revisited: using ribosomal proteins to resolve deep branching dinoflagellate clades. *Molecular Phylogenetics and Evolution*, **70**: 314–322.

Bergh, R.S. (1881). Der Organismus der Cilioflagellaten. Eine phylogenetische Studie. *Morphologisches Jahrbuch*, **7**: 177–288, pl. 12–16.

Bhaud, Y., Soyer-Gobillard, M.O. & Salmon, J.M. (1988). Transmission of gametic nuclei through a fertilization tube during mating in a primitive dinoflagellate, *Prorocentrum micans* Ehr. *Journal of Cell Science*, **89**: 197–206.

Biecheler, B. (1952). Recherches sur les Peridiniens. *Bulletin Biologique de la France et de la Belgique*, **Suppl**. 36: 1–149.

Braarud, T. & Rossavik, E. (1951). Observations on the marine dinoflagellate *Prorocentrum micans* Ehrenb. in culture. *Avhandl. Norske Videnskaps-Akad. Oslo. I. Mat. Naturv Kl.*, **1**: 3–18.

Braarud, T. & Heimdal, B. (1970). Brown waters on the Norwegian coast in autumn 1966. *Nytt Magasin for Botanik*, **17**: 91–97.

Brand, L.E. (1985). Low genetic variability in reproduction rates in populations of *Prorocentrum micans* Ehrenb. (Dinophyceae) over Georges Bank. *Journal of Experimental Marine Biology and Ecology*, **88**: 55–65.

Bursa, A.S. (1959). The genus *Prorocentrum* Ehrenberg. Morphodynamics, protoplasmic structure. *Canadian Journal of Botany*, **37**: 1–31.

Caroppo, C., Pagliari, P., Azzaro, F., Miserocchi, S. & Azzaro, M. (2017). Late summer phytoplankton blooms in the changing polar environment of the Kongsfjorden (Svalbard, Arctic). *Cryptogamie Algologie*, **38**: 53–72.

Cassie, V. (1981). Non-toxic blooms of *Prorocentrum micans* (Dinophyceae) in the Karanea Bight. *New Zealand Journal of Marine and Freshwater Research*, **15**: 181–184.

Cohen-Fernandez, E.J., Del Castillo, E.M., Ugarte, I.H.S. & Pedroche, F.F. (2006). Contribution of external morphology in solving a species complex: the case of *Prorocentrum sigmoides* (Dinoflagellata) from the Mexican Pacific Coast. *Phycological Research*, **54**: 330–340.

Cohen-Fernandez, E.J., Pedroche, F.F., Palacios, M.R., Hernandez, S.A. & Del Castillo, E.M. (2010). Molecular phylogeny of *Prorocentrum* (Dinoflagellata) from the Pacific coast of Mexico based on the parsimony analysis of fragments of LSUrDNA and SSUrDNA. *International Journal of Plant Physiology and Biochemistry*, **2**: 29–37.

Day, J.G., Pröschold, T., Friedl, T., Lorenz, M. & Silva, P.C. (2010). Conservation of microalgal type material: approaches needed for 21st century science. *Taxon*, **59**: 3–6.

Dodge, J.D. (1975). The Prorocentrales (Dinophyceae). II. Revision of the taxonomy within the genus *Prorocentrum. Botanical Journal of the Linnean Society*, **71**: 103–125.

Dodge, J.D. (1982). *The Dinoflagellates of the British Isles*. Her Majesty's Stationery Office, London.

Dodge, J.D. & Bibby, B.T. (1973). The Prorocentrales (Dinophyceae) I. A comparative account of fine structure in the genera *Prorocentrum* and *Exuviella. Botanical Journal of the Linnean Society*, **67**: 175–187.

Eggersdorfer, B. & Häder, D.P. (1991). Phototaxis, gravitaxis and vertical migrations in the marine dinoflagellate *Prorocentrum micans. FEMS Microbiology Letters*, **85**: 319–326.

Ehrenberg, C.G. (1835). Dritter Beitrag zur Erkenntnis großer Organisation in der Richtung des kleinsten Raumes. *Abhandlungen der Königlichen Akademie der Wissenschaften in Berlin 1833: Physikalische Klasse*, 145–336.

Ehrenberg, C.G. (1836). Über das Leuchten des Meeres. *Abhandlungen der Königlichen Akademie der Wissenschaften in Berlin 1834*, 411–575, tabs 411–412.

Faust, M.A., Larsen, J. & Moestrup, O. (1999). Leaflet no 184. Potentially toxic phytoplankton 3. Genus *Prorocentrum* (Dinophyceae). In *ICES Identification Leaflets for Plankton* (Lindley, J.A., editor), 1–24. International Council for the Exploration of the Sea, Copenhagen.

Fensome, R.A., Taylor, F.J.R., Norris, G., Sarjeant, W.A.S., Wharton, D.I. & Williams, G.L. (1993). A classification of living and fossil dinoflagellates. *Micropaleontology, Special Publication*, **7**: 1–351.

Gómez, F., Qiu, D. & Lin, S. (2017). The synonymy of the toxic dinoflagellates *Prorocentrum mexicanum* and *P. rhathymum* and the description of *P. steidingerae* sp. nov. (Prorocentrales, Dinophyceae). *Journal of Eukaryotic Microbiology*, **64**: 668–677.

Gottschling, M. & Plötner, J. (2004). Secondary structure models of the nuclear Internal Transcribed Spacer regions and 5.8S rRNA in Calciodinelloideae (Peridiniaceae) and other dinoflagellates. *Nucleic Acids Research*, **32**: 307–315.

Gottschling, M., Söhner, S., Zinßmeister, C., John, U., Plötner, J., Schweikert, M., Aligizaki, K. & Elbrächter,

M. (2012). Delimitation of the Thoracosphaeraceae (Dinophyceae), including the calcareous dinoflagellates, based on large amounts of ribosomal RNA sequence data. *Protist*, **163**: 15–24.

Gu, H., Kirsch, M., Zinßmeister, C., Söhner, S., Meier, K.J.S., Liu, T. & Gottschling, M. (2013). Waking the dead: morphological and molecular characterization of extant †*Posoniella tricarinelloides* (Thoracosphaeraceae, Dinophyceae). *Protist*, **164**: 583–597.

Han, M.S., Wang, P., Kim, J.H., Cho, S.Y., Park, B.S., Kim, J.H., Katano, T. & Kim, B.H. (2016). Morphological and molecular phylogenetic position of *Prorocentrum micans* sensu stricto and description of *Prorocentrum koreanum* sp. nov. from southern coastal waters in Korea and Japan. *Protist*, **167**: 32–50.

Hasle, G.R. (1950). Phototactic vertical migration in marine dinoflagellates. *Oikos*, **2**: 162–175.

Henrichs, D.V., Scott, P., Steidinger, K., Errera, R.M., Abraham, A. & Campbell, L. (2013). Morphology and phylogeny of *Prorocentrum texanum* sp. nov. (Dinophyceae): a new toxic dinoflagellate frim the Gulf of Mexico coastal waters exhibiting two distinct morphologies. *Journal of Phycology*, **49**: 143–155.

Hernández-Becerril, D.U., Altamirano, R.C. & Alonso, R. (2000). The dinoflagellate genus *Prorocentrum* along the coasts of the Mexican Pacific. *Hydrobiologia*, **418**: 111–121.

Herrera-Sepúlveda, A., Medlin, L., Murugan, G., Sierra-Beltran, A.P., Cruz-Villacorta, A.A. & Hernandez-Saavedra, N.Y. (2015). Are *Prorocentrum hoffmanianum* and *Prorocentrum belizeanum* (Dinophyceae, Prorocentrales), the same species? An integration of morphological and molecular data. *Journal of Phycology*, **51**: 173–188.

Hoppenrath, M., Elbrächter, M. & Drebes, G. (2009). *Marine Phytoplankton*. E. Schweizerbart´sche Verlagsbuchhandlung, Stuttgart, Germany.

Hoppenrath, M., Chomérat, N., Horiguchi, T., Schweikert, M., Nagahama, Y. & Murray, S. (2013). Taxonomy and phylogeny of the benthic *Prorocentrum* species (Dinophyceae) – a proposal and review. *Harmful Algae*, **27**: 1–28.

Jacobson, D.M. & Anderson, D.M. (1996). Widespread phagocytosis of ciliates and other protists by mixotrophic and heterotrophic thecate dinoflagellates. *Journal of Phycology*, **32**: 279–285.

Jeong, H.J., Yoo, Y.D., Park, J.Y., Song, J.Y., Kim, S.T., Lee, S.H., Kim, K.Y. & Yih, W.H. (2005). Feeding by phototrophic red-tide dinoflagellates: five species newly revealed and six species previously known to be mixotrophic. *Aquatic Microbial Ecology*, **40**: 133–150.

Jin, Q., Dong, S. & Wang, C. (2005). Allelopathic growth inhibition of *Prorocentrum micans* (Dinophyta) by *Ulva pertusa* and *Ulva linza* (Chlorophyta) in laboratory cultures. *European Journal of Phycology*, **40**: 31–37.

Kain, J.M. & Fogg, G.E. (1960). Studies on the growth of marine phytoplankton. III. *Prorocentrum micans* Ehrenberg. *Journal of the Marine Biological Association of the United Kingdom*, **39**: 33–50.

Keller, M.D., Selvin, R.C., Claus, W. & Guillard, R.R.L. (1987). Media for the culture of oceanic ultraphytoplankton. *Journal of Phycology*, **23**: 633–638.

Kretschmann, J., Žerdoner Čalasan, A., Kusber, W.-H. & Gottschling, M. (2018). Still curling after all these years: *Glenodinium apiculatum* Ehrenb. (Peridiniales, Dinophyceae) repeatedly found at its type locality in Berlin (Germany). *Systematics and Biodiversity*, **16**: 200–209.

Kretschmann, J., Elbrächter, M., Zinßmeister, C., Söhner, S., Kirsch, M., Kusber, W.-H. & Gottschling, M. (2015). Taxonomic clarification of the dinophyte *Peridinium acuminatum* Ehrenb., ≡ *Scrippsiella acuminata*, comb. nov. (Thoracosphaeraceae, Peridiniales). *Phytotaxa*, **220**: 239–256.

Krock, B., Tillmann, U., John, U. & Cembella, A.D. (2008). LC-MS/MS On Board Ship – tandem mass spectrometry in the search for phycotoxins and novel toxigenic plankton from the North Sea. *Analytical and Bioanalytical Chemistry*, **392**: 797–803.

Kusber, W.H., Elbrächter, M. & Jahn, R. (2005). Algae of the Ehrenberg collection – 2. The type specimens of two dinoflagellate names published by C.G. Ehrenberg. *Willdenowia*, **35**: 205–210.

Lebour, M.V. (1925). *The Dinoflagellates of the Northern Seas*. The Marine Biological Association, UK, Plymouth.

Lin, S., Zhang, H. & Jiao, N. (2006). Potential utility of mitochondrial cytochrome b and its mRNA editing in resolving closely related dinoflagellates: a case study of *Prorocentrum* (Dinophyceae). *Journal of Phycology*, **42**: 646–654.

Lohmann, H. (1908). Untersuchungen zur Feststellung des vollständigen Gehaltes des Meeres an Plankton. *Wissenschaftliche Meeresuntersuchungender Kommission zur wissenschaftlichen Untersuchung der deutschen Meere (Kiel)*, **10**: 129–370.

Mahoney, J.B. & McLaughlin, J.J.A. (1977). The association of phytoflagellate blooms in lower New York bay with hypertrophication. *Journal of Experimental Marine Biology and Ecology*, **28**: 53–65.

McLachlan, J.L., Boalch, G.T., & Jahn, R. (1997). Reinstatement of the genus *Exuviaella* (Dinophyceae, Prorocentrophycidae) and an assessment of *Prorocentrum lima*. *Phycologia*, **36**: 38–46.

Murray, S., Ip, C.L., Moore, R., Nagahama, Y. & Fukuyo, Y. (2009). Are prorocentroid dinoflagellates monophyletic? A study of 25 species based on nuclear and mitochondial genes. *Protist*, **160**: 245–264.

Nagahama, Y., Murray, S., Tomaru, A. & Fukuyo, Y. (2011). Species boundaries in the toxic dinoflagellate *Prorocentrum lima* (Dinophyceae, Prorcentrales), based on morphological and phylogenetic characters. *Journal of Phycology*, **47**: 178–189.

Okolodkov, J.B. (1998). A checklist of dinoflagellates recorded from the Russian Arctic Seas. *Sarsia*, **83**: 267–292.

Omura, T., Iwataki, M., Borja, V.M., Takayama, H. & Fukuyo, Y. (2012). *Marine Phytoplankton of the Western Pacific*. Kouseisha Kouseikaku, Tokyo.

Orr, R., Murray, S.A., Stüken, A., Rhodes, L. & Jakobsen, K. S. (2012). When naked became armored: an eight-gene phylogeny reveals monophyletic origin of theca in dinoflagellates. *PLoS ONE*, **7**: e50004.

Paulmier, G. (1992). Catalogue illustré des microphytes plantonique et benthique des cotes normandes. *Rapports internes de la Direction des Resources Vivantes de L`IFREMER*.

Paulsen, O. (1907). The Peridiniales of the Danish Waters. *Meddelelser fra Kommissionen for Havundersogelser Serie: Plankton*, **1**: 1–26.

Pinto, J.D.S. & Silva, E.D.S. (1956). The toxicity of *Cardium edule* L. and its possible relation to the dinoflagellate *Prorocentrum micans*. *Notas e estudos di Instituto do Biologia Marítima*, **12**: 1–20.

Pitcher, G.C. & Calder, D. (2000). Harmful algal blooms of the southern Benguela Current: a review and appraisal of monitoring from 1989 to 1997. *South African Journal of Marine Science*, **22**: 255–271.

Roberts, K.R., Heimann, K. & Wetherbee, R. (1995). The flagellar apparatus and canal structure in *Prorocentrum micans* (Dinophyceae). *Phycologia*, **34**: 313–322.

Schnepf, E. & Winter, S. (1990). A microtubular basket in the armoured dinoflagellate *Prorocentrum micans* (Dinophyceae). *Archiv für Protistenkunde*, **138**: 89–91.

Shankle, A.M., Mayali, X. & Franks, P.J.S. (2004). Temporal patterns in population genetic diversity of *Prorocentrum micans* (Dinophyceae). *Journal of Phycology*, **40**: 239–247.

Shumway, S.E. (1990). A review of the effects of algal blooms on shellfish and aquaculture. *Journal of the World Aquaculture Society*, **21**: 65–104.

Silva, E.S. (1959). Some observations on marine dinoflagellate cultures I. *Prorocentrum micans* Ehr. and *Gyrodinium* sp. *Notas e Estudos di Instituto de Biologia Marítima, Lisboa*, **21**: 1–15.

Stein, F. (1883). *Der Organismus der Infusionsthiere nach eigenen Forschungen in systematischer Reihenfolge bearbeitet. III. Abt. II. Hälfte. Der Organismus der Arthrodelen Flagellaten*. W. Engelmann, Leipzig.

Taylor, F.J.R. (1976). Dinoflagellates from the International Indian Ocean 1976 Expedition. *Bibliotheca Botanica*, **132**: 1–234.

Taylor, F.J.R. (1980). On dinoflagellate evolution. *BioSystems*, **13**: 65–108.

Tillmann, U., Hoppenrath, M., Gottschling, M., Kusber, W.H. & Elbrächter, M. (2017). Plate pattern clarification of *Heterocapsa triquetra* sensu Stein (Heterocapsaceae, Dinophyceae). *Journal of Phycology*, **53**: 1305–1324.

Uchida, T. (1977). Excretion of a diatom-inhibitory substance by *Prorocentrum micans* Ehrenberg. *Japanese Journal of Ecology*, **27**: 1–4.